Reprinted from
*Journal of Imaging Science and Technology*® 62(4): 040408-1–040408-6, 2018.


# Particle Transport in Microchannels

**L. Pekker**
*FUJIFILM Dimatix Inc., Lebanon NH 03766, USA*
*E-mail: leonid.pekker@fujifilm.com*

**Abstract.** *In this article, the author describes a set of models of particle transport in microchannels that has been recently developed at FUJIFILM Dimatix for design and optimization inkjet print heads. The models are used to estimate the modes of particle transport in horizontal channels, the times for particles to settle at the bottom of a channel, and the fluidization flow velocity. The Rouse number is commonly used to estimate the mode of sediment transport in horizontal turbulent flow with large Reynolds number. However, in microchannels such as in modern inkjet systems, the liquid flows are usually laminar. In this article, the author uses a modified Rouse number that is expanded to the case of weakly turbulent and laminar flows. To illustrate the applicability of the modified Rouse number, he applies it to the transport of pigment particles in a horizontal channel in the FUJIFILM inkjet print head and compares theoretical results with experimental observations. In the article, he also constructs a model to estimate two settling times in rectangular channels: the time of formation of a monolayer of particles at the bottom of a channel and the required time for all particles to settle at the channel bottom. In design and optimization of a print jet head, it is also important to know the critical fluidization flow velocity of the ink to prevent sedimentation of ink pigment particles in vertical channels. In this article, the author constructs a simple model to estimate the maximum fluidization flow velocity as well. The modified Rouse number constructed in this article, as well as presented models, can be used in other applications as well.* 
[DOI: 10.2352/J.ImagingSci.Technol.2018.62.4.040408]

## 1. SEDIMENT TRANSPORT IN HORIZONTAL MICROCHANNELS

In 1937, Hunter Rouse introduced a characteristic non-dimensional scale parameter [1], which later was named the Rouse number,

$$P = \frac{v_t}{u_* \kappa}, \tag{1}$$

that describes the modes of sediment transported in turbulent horizontal flows. In this equation, $v_t$ is the free fall terminal (settling) velocity of a sediment particle in the fluid, $\kappa = 0.4$ is the Karman constant calculated for turbulent flow, and $u_*$ is the boundary shear velocity, determined as

$$u_* = \sqrt{\tau/\rho_f}, \tag{2}$$

where $\tau$ is the shear stress of the fluid at the bottom (at the sediment bed) and $\rho_f$ is the mass density of the fluid. Table I presents the transport mode of sediment versus the Rouse number [2]. An approximate formula for the terminal velocity of grains [3] is

$$v_t = \frac{gD^2(\rho_p - \rho_f)}{C_1\mu + \sqrt{0.75C_2(\rho_p - \rho_f)\rho_f g D^3}}, \tag{3}$$

with coefficients $C_1$ and $C_2$ from Table II [3]. In Eq. (3), $C_1$ and $C_2$ are the creepy and turbulent drag coefficients respectively; $g$ is the Earth's gravitation acceleration; $D$ is the characteristic diameter of a particle; $\rho_p$ is the mass density of a particle; and $\mu$ is the fluid viscosity.

Since, in turbulent flow, $u_*$ is proportional to the lift velocity of a particle at the sediment bed, Table I has perfect physical sense. Indeed, for large $P$, where the deposition rate of particles due to the gravity prevails over the particle lift, the sediment is transported as a bed load (in bed load mode); for small $P$, where the lift velocity of the particles is about the particle terminal velocity, the particles are suspended in the flow and, therefore, the sediment is transported in the suspension mode; for very small $P$, where the particle lift velocity is much larger than the deposition rate of particles, the sediment is transported in the wash load mode. On the other hand, there should be a critical Rouse number that corresponds to a threshold for initiating the sediment motion; this is very important to know when designing microchannels to transport liquids with particles as, for example, in the case of inkjet systems. This threshold is described by the widely used Shields diagram [4, 5], which, unlike the Rouse number, is applicable for a large range of Reynolds numbers, including laminar flows as well, Figure 1.

To correlate the Rouse number with the Shields diagram, we will reformulate the Rouse number in terms of the Shields diagram [6]. In the Shields diagram, Fig. 1, the particle boundary Reynolds number $Re_*$ and the particle shear stress $\tau_*$ are determined as

$$Re_* = \frac{D}{\mu}\sqrt{\tau\rho_f} \tag{4}$$

and

$$\tau_* = \frac{\tau}{Dg(\rho_p - \rho_f)}. \tag{5}$$

By substituting Eqs. (2) and (3) into Eq. (1) and then using Eqs. (4) and (5), Eq. (1) can be reduced to the following

Received Mar. 21, 2018; accepted for publication June 7, 2018; published online July 31, 2018. Associate Editor: Frits Dijksman.
1062-3701/2018/62(4)/040408/6/$25.00

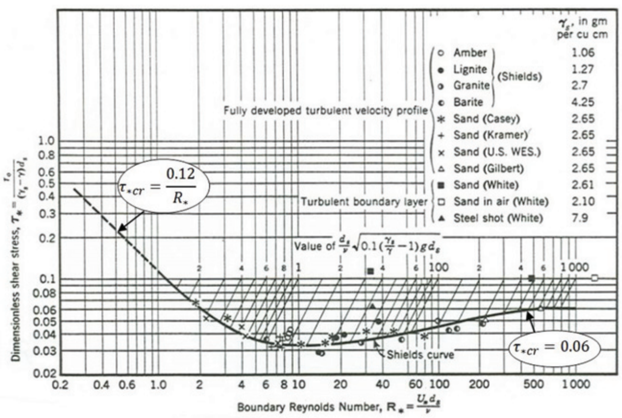


Figure 1. The Shields diagram curve. In this diagram, $R_*$ corresponds to $Re_*$, $\tau_O \to \tau$, $\gamma_S \to g\rho_p$, $\gamma \to g\rho_f$, $U_* \to u_*$, $d_s \to D$, and $\nu \to \mu/\rho_f$.

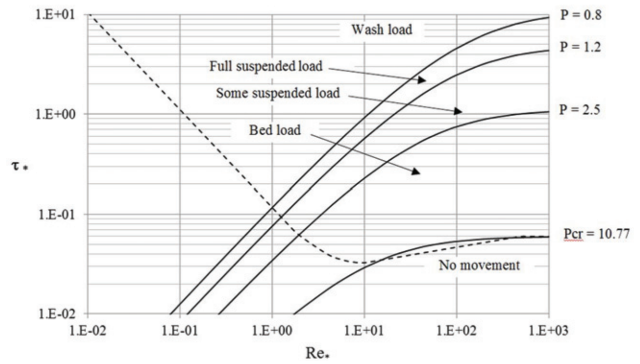


Figure 2. The Shields diagram curve versus the Rouse number. The broken line is the Shields diagram curve (Fig. 1) and the solid lines are Rouse number curves at given $P$, Eq. (9), for ultra-angular grains, Table II.

**Table I.** Modes of sediment transport [2].

| Mode of transport | Rouse number |
|---|---|
| Bed load | $P > 2.5$ |
| Suspended load: 50% suspended | $1.2 < P < 2.5$ |
| Suspended load: 100% suspended | $0.8 < P < 1.2$ |
| Wash load | $P < 0.8$ |

**Table II.** Coefficients for settling velocity of grains [3].

| Constant | Smooth sphere | Natural grains: sieve diameters | Natural grains: nominal diameters | Limit for ultra-angular grains |
|---|---|---|---|---|
| $C_1$ | 18 | 18 | 20 | 24 |
| $C_2$ | 0.4 | 1.0 | 1.1 | 1.2 |

form:

$$P = \frac{1}{\kappa C_1}\left(\frac{Re_*}{\tau_*}\right)\left(1 + \sqrt{\frac{0.75C_2}{C_1^2}}\left(\frac{Re_*}{\sqrt{\tau_*}}\right)\right)^{-1}. \quad (6)$$

Asymptotic solutions of Eq. (6) are

$$\tau_*(Re_* \to \infty) = \frac{4}{3C_2(\kappa P)^2} \quad (7)$$

and

$$\tau_*(Re_* \to 0) = \frac{Re_*}{\kappa C_1 P}. \quad (8)$$

Solving Eq. (6) for $\tau_*$, we obtain that $\tau_*$ can be expressed in terms of $Re_*$ and $P$ as follows:

$$\tau_* = \left(-\left(\frac{0.75C_2Re_*^2}{4C_1^2}\right)^{0.5} + \left(\frac{0.75C_2Re_*^2}{4C_1^2} + \frac{Re_*}{\kappa C_1 P}\right)^{0.5}\right)^2. \quad (9)$$

The Shields curve also has two asymptotes, Fig. 1,

$$\tau_{*\mathrm{cr}}(Re_* \to \infty) = 0.06, \quad (10)$$

and

$$\tau_{*\mathrm{cr}}(Re_* \to 0) = \frac{0.12}{Re_*}. \quad (11)$$

It should be stressed that from the experimental data shown in the Shields diagram [4], it is difficult to say how far the Shield's asymptote in Fig. 1 can be extended for small $Re_*$. In the Appendix, we suggest an explanation why the Shields asymptote observed for relatively large $Re_*$, Fig. 1, can be extended to $Re_* \ll 1$ where the experimental data are absent.

To match the Rouse number and the Shields diagram, we introduce the critical value of the Rouse number, $P_{\mathrm{cr}}$, that yields the same $\tau_*$ as the Shields diagram at $Re_* \gg 1$ and corresponds to the threshold of initiation of the sediment motion at the bed. Setting Eqs. (7) and (10) equal to each other, we obtain

$$P_{\mathrm{cr}} = \frac{11.79}{\sqrt{C_2}}. \quad (12)$$

In Eq. (12), we have taken into account that the Karman constant is equal to 0.4.

Figure 2 shows the Shields curve, $\tau_{*\mathrm{cr}}(Re_*)$, and curves of $\tau_*(Re_*)$ calculated by Eq. (9) for different modes of sediment transport in the case of ultra-angular grains; $C_1$ and $C_2$ are taken from Table II. As one can see from Fig. 2, in the case of the threshold of initiation of the sediment motion mode, $\tau_*(P_{\mathrm{cr}}, Re_*)$ is in good agreement with the Shields diagram when $Re_* > 10$. However, with a decrease in $Re_*$, $\tau_*(P_{\mathrm{cr}}, Re_*)$ sharply diverges from the Shields diagram. For other sediment transport modes, $\tau_*$ has no sense for small $Re_*$ as well. This is so because Eq. (1) is applicable for turbulent flows only, for large $Re_*$.

To expand the Rouse number to small $Re_*$ and at the same time to preserve the asymptote of $\tau_*(P_{\mathrm{cr}}, Re_* \to \infty)$, Eq. (7) with $P = P_{\mathrm{cr}}$, we will modify the Rouse number by using $\tilde{\kappa}$,

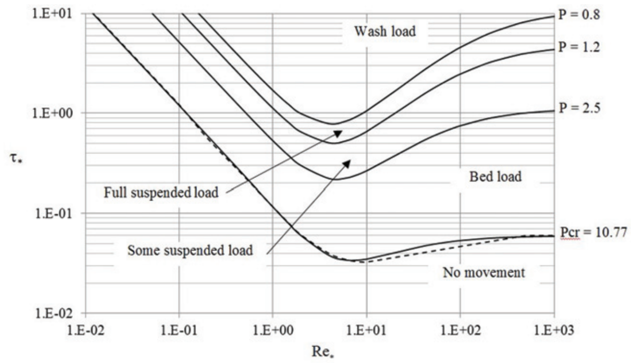


Figure 3. The Shields diagram curve versus the modified Rouse number. The broken line is the Shields diagram curve (Fig. 1) and the solid lines are the modified Rouse number curves at given $P$, Eq. (14), for ultra-angular grains, Table II.

$$\frac{1}{\tilde{\kappa}} = \frac{1}{\kappa} + \frac{0.12 C_1 P_{\text{cr}}}{Re_*^2}, \tag{13}$$

for $\kappa$ in Eq. (9); this yields

$$\tau_* = \left( -\left( \frac{0.75 C_2 Re_*^2}{4C_1^2} \right)^{0.5} + \left( \frac{0.75 C_2 Re_*^2}{4C_1^2} + \frac{Re_*}{0.4 C_1 P} + \frac{0.12 P_{\text{cr}}}{P Re_*} \right)^{0.5} \right)^2. \tag{14}$$

The substitution of $\tilde{\kappa}$ for $\kappa$ in Eqs. (7) and (8) shows that for $P = P_{\text{cr}}$ the asymptotes of Eqs. (14) for $Re_* \gg 1$ and $Re_* \ll 1$ indeed coincide with Eqs. (10) and (11) correspondingly. Figure 3 demonstrates the excellent agreement between the Shields diagram curve and $\tau_*(P_{\text{cr}}, Re_*)$.

To illustrate the applicability of the modified Rouse number, we applied it to the transport of sediment in a channel of a Fuji Dimatix SG 1024 inkjet head and compared theoretical results with experimental observations. Table III presents the combined input and output parameters of the model for a channel of this print head for two ink flows, $2.71 \cdot 10^{-8}$ and $5.646 \cdot 10^{-7}$ m$^3$/s, and Figure 4 presents the results of the calculations in the Shields diagram variables. In this calculation, the shear stress at the bottom was calculated assuming Poiseuille's law, which is reasonable for this particular application. As one can see from this figure, in the case of small flow, the sediment transport is in no movement mode, while in the case of large flow, it is in wash load mode. The experimental work with this type of print head showed that, for the ink flow of $2.71 \cdot 10^{-8}$ m$^3$/s, all nozzles of the print head were completely blocked by pigment particles and the print head could not be recovered; this experimental result corresponds to the case of "small flow" in Fig. 4. However, for the ink flow of $5.646 \cdot 10^{-7}$ m$^3$/s, the print head worked normally and the particles were transported through this channel; this regime corresponds to the case of "large flow" in Fig. 4. Thus, the experimental findings support the theoretical model.

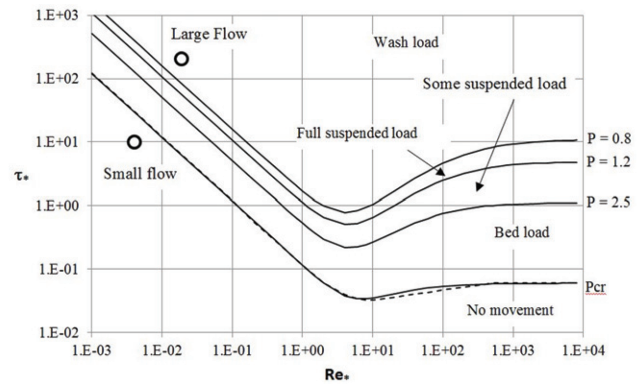


Figure 4. $Re_*$ and $\tau_*$ calculated for the large and small flows. The parameters of the model are presented in Table III; the broken line corresponds to the Shields diagram curve.

**Table III.** Combined input and calculated parameters of the model.

| Input parameter | Small flow | Large flow |
|---|---|---|
| Particle diameter, $D$ (m) | 5.0E-06 | 5.0E-06 |
| Particle density, $\rho_p$ (kg/m$^3$) | 1320 | 1320 |
| Fluid density, $\rho_w$ (kg/m$^3$) | 1000 | 1000 |
| Viscosity (Pa · s) | 0.015 | 0.015 |
| $C_1$ | 24 | 24 |
| $C_2$ | 1.2 | 1.2 |
| Flow, $Q$ (m$^3$/s) | 2.71E-8 | 5.646E-7 |
| Radius of the pipe, $R$ (m) | 1.5E-03 | 1.5E-03 |
| Output parameter | | |
| Shear stress, $\tau$ (Pa) | 0.153 | 3.194 |
| Boundary Reynolds number, $Re_*$ | 0.004 | 0.019 |
| Boundary shear stress, $\tau_*$ | 9.770 | 203.518 |
| $P_{\text{cr}}$ | 10.76 | 10.76 |
| Shield's shear stress, $\tau_{*P=P_{\text{cr}}}$ | 29.070 | 6.368 |
| Shear stress some suspension, $\tau_{*P=2.5}$ | 125.239 | 27.438 |
| Shear stress full suspension, $\tau_{*P=1.2}$ | 260.916 | 57.165 |
| Shear stress wash load, $\tau_{*P=0.8}$ | 391.375 | 85.748 |
| Resuspension? | **No movement** | **Wash load** |

## 2. SEDIMENT SETTLING TIME IN A RECTANGULAR CHANNEL

Figure 5 illustrates the model of settling particles considered in the calculation. In the model, $\tau_{s\text{-layer}}$ is the characteristic time of formation of a monolayer of particles at the bottom of the channel and $\tau_{s\text{-full}}$ is the characteristic time for settling of all particles at the bottom, Fig. 5. The porosity $\Phi$ is determined as the volume fraction of the liquid in the liquid–particle mixture and $\Phi_{\text{pack}}$ is the packed porosity of particles settled at the bottom of the channel, Fig. 5.

The total volume of particles per unit area at the bottom of the channel at time $t = 0$, Fig. 5, can be written as

$$V_p = H_0(1 - \Phi), \tag{15}$$

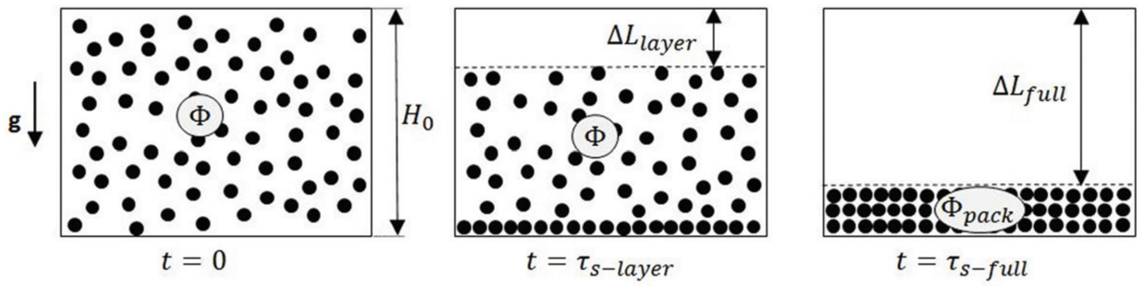


Figure 5. Schematics of the model for calculating the settling times. Here in the calculation. Here, $H_0$ is the height of the rectangular channel, $t$ is time, $\Phi$ is the porosity of the liquid–particle mixture, and $\Phi_{\mathrm{pack}}$ is the packed porosity of particles that have settled at the bottom of the channel.

where $H_0$ is the height of the rectangular channel. Assuming in the model that the porosity of the mixture does not change with time, equations for $\Delta L_{\mathrm{layers}}$ and $\Delta L_{\mathrm{full}}$, Fig. 5, can be written as

$$V_p = D(1-\Phi_{\mathrm{pack}}) + (H_0 - \Delta L_{\mathrm{layer}})(1-\Phi), \quad (16)$$
$$V_p = (H_0 - \Delta L_{\mathrm{full}})(1-\Phi_{\mathrm{pack}}), \quad (17)$$

where, as in Section 1, $D$ is the characteristic diameter of the particles. Since, in the model, the porosity of the mixture is assumed to be constant and independent of time (Fig. 5), the settling rate of the particles, $v_s$, is also constant and independent of time. This leads to the following expressions for the settling times:

$$\tau_{s\text{-layer}} = \frac{\Delta L_{\mathrm{layer}}}{v_s} \quad \text{and} \quad \tau_{s\text{-full}} = \frac{\Delta L_{\mathrm{full}}}{v_s}. \quad (18)$$

By combining Eqs. (15)–(18), we obtain

$$\tau_{s\text{-layer}} = \frac{D(1-\Phi_{\mathrm{pack}})}{v_s(1-\Phi)} \quad \text{and} \quad \tau_{s\text{-full}} = \frac{H_0(\Phi-\Phi_{\mathrm{pack}})}{v_s(1-\Phi_{\mathrm{pack}})}. \quad (19)$$

Now, we estimate the settling rate of the sediment. Following [7], the pressure gradient, or drag force, on the stationary bed of particles (porous media in [7]) can be written as

$$\nabla P = \frac{7}{4}\rho_f \frac{u_f^2(1-\Phi)}{D\Phi^3} + 150\frac{(1-\Phi)\mu u_f}{\Phi^3 D^2}, \quad (20)$$

where $u_f$ is the flow velocity of the liquid entering the porous "block," Figure 6.

The total force pushing the liquid through the porous block, Fig. 6, is equal to the total drag force applied to the bed of stationary particles and can be written as

$$F_{\mathrm{drag}} = SL\left(\frac{7}{4}\rho_f \frac{u_f^2(1-\Phi)}{D\Phi^3} + 150\frac{(1-\Phi)^2\mu u_f}{\Phi^3 D^2}\right). \quad (21)$$

By setting Eq. (21) equal to the gravitational force minus the buoyancy force applied to the bed of particles, $g(\rho_p - \rho_f)(1-\Phi)SL$, we obtain an equation for the critical liquid flow velocity, $u_{f,\mathrm{cr}}$, for the fluidization of the bed of particles

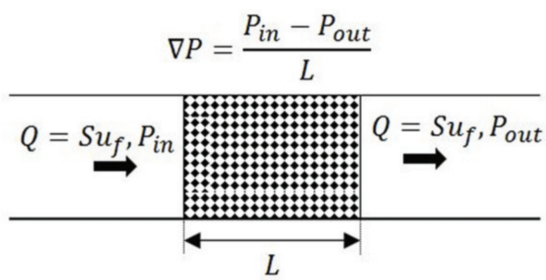


Figure 6. Schematics of the model [7]. Here, $S$ and $L$ are the cross-section and the length of a porous block respectively, $Q$ is the liquid flow through the block, $u_f$ the flow velocity of the fluid entering the block, and $P_{\mathrm{in}}$ and $P_{\mathrm{out}}$ are correspondingly the inlet and outlet liquid pressures at the block.

in vertical channel flow,

$$\left(\frac{7}{4}\rho_f \frac{u_{f,\mathrm{cr}}^3}{D\Phi^3} + 150\frac{(1-\Phi)\mu u_{f,\mathrm{cr}}}{\Phi^3 D^2}\right) = g(\rho_p - \rho_f). \quad (22)$$

As follows from Fig. 6, the liquid flow velocity in porous media is equal to $u_f/\Phi$. Since, in our case, Fig. 5, in the sediment coordinate system, the liquid velocity is equal to $v_s$, the relationship between $v_s$ and $u_{f,\mathrm{cr}}$ is

$$u_{f,\mathrm{cr}} = v_s\Phi. \quad (23)$$

It is worth noting that Eq. (23) yields $u_{f,\mathrm{cr}} \to V_s$ if $\Phi \to 1$; this makes perfect sense because the case of $\Phi = 1$ corresponds to the case of a free falling particle in an infinitely large liquid medium.

On substituting Eq. (23) into Eq. (22), we obtain the following quadratic equation for $v_s$:

$$v_s^2 + v_s\frac{600\mu(1-\Phi)}{7D\rho_f\Phi} - \frac{4D\Phi g(\rho_p-\rho_f)}{7\rho_f} = 0. \quad (24)$$

Solving this equation for $v_s$, we obtain

$$v_s = -\left(\frac{300}{7}\frac{\mu(1-\Phi)}{D\rho_f\Phi}\right) + \left(\left(\frac{300}{7}\frac{\mu(1-\Phi)}{D\rho_f\Phi}\right)^2 + \frac{4D\Phi g(\rho_p-\rho_f)}{7\rho_f}\right)^{1/2}. \quad (25)$$

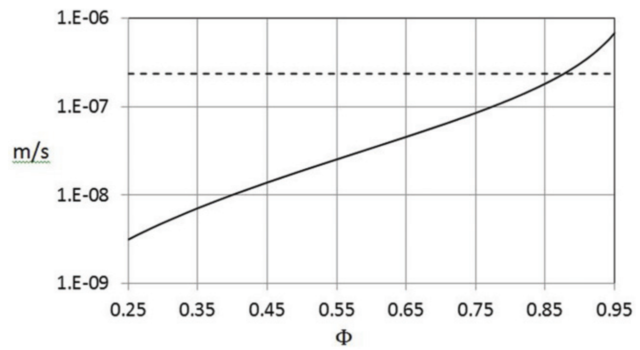


Figure 7. $v_s(\Phi)$ from Eq. (25) (solid lines) and $v_t$ from Eq. (3) (dashed line). The liquid and particle parameters are from Table IV.

**Table IV.** Combined input and calculated parameters of the model.

| Input parameter | Input data |
|---|---|
| $H_0$ (m) | 3.00E-03 |
| $D$ (m) | 5.00E-06 |
| $\rho_p$ (kg/m$^3$) | 1352 |
| $\rho_f$ (kg/m$^3$) | 1000 |
| $\mu$ (Pa · s) | 1.52E-02 |
| $\Phi$ — porosity | 0.700 |
| $\Phi_{pack}$ — porosity | 0.240 |
| $C_1$ | 24 |
| $C_2$ | 1.2 |
| **Output parameter** | **Output data** |
| $v_s$ (m/s) | 6.18E-08 |
| $\tau_{full}$ (s) | 2.94+04 |
| $\tau_{layer}$ (s) | 2.05+02 |

Since the sediment deposition velocity cannot be larger than the terminal velocity of a particle, $v_t$ in Eq. (3), we use the following formula for the particle settling rate:

$$v_s = \min\left\{ -\left(\frac{300}{7}\frac{\mu(1-\Phi)}{D\rho_f\Phi}\right) + \left(\left(\frac{300}{7}\frac{\mu(1-\Phi)}{D\rho_f\Phi}\right)^2 + \frac{4D\Phi g(\rho_p-\rho_f)}{7\rho_f}\right)^{1/2}, \frac{gD^2(\rho_p-\rho_f)}{C_1\mu+\sqrt{0.75C_2(\rho_p-\rho_f)\rho_f gD^3}} \right\}. \tag{26}$$

Substitution of Eq. (26) into Eqs. (18) yields $\tau_{s\text{-layer}}$ and $\tau_{s\text{-full}}$.

An example of input and output parameters for the settling time model is presented in Table IV.

Figure 7 shows $v_s$ versus $\Phi$ from Eq. (25) and $v_t$ from Eq. (3) for fluid and particle parameters from Table IV. As follows from this figure and Eq. (26), for $\Phi > 0.88$, the particle settling rate is given by Eq. (3).

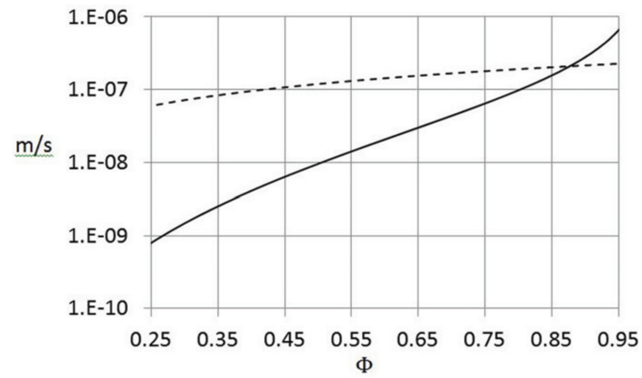


Figure 8. $u_{f,\mathrm{cr}}(\Phi)$ from Eq. (27) (solid lines) and $\Phi v_t$ from Eq. (3) (dashed line). The liquid and particle parameters are from Table V.

## 3. FLUIDIZATION FLOW VELOCITY (VERTICAL CHANNEL FLOW)

A solution of Eq. (22) for $u_{f,\mathrm{cr}}$ yields the following expression for the critical liquid fluidization velocity for the bed of particles with porosity $\Phi$:

$$u_{f,\mathrm{cr}} = -\frac{300(1-\Phi)\mu}{7D\rho_f} + \left(\left(\frac{300(1-\Phi)\mu}{7D\rho_f}\right)^2 + \frac{4\Phi^3 g(\rho_p-\rho_f)D}{7\rho_f}\right)^{1/2}. \tag{27}$$

Since, as has been mentioned in Section 2, the liquid flow velocity in porous media is equal to $u_f/\Phi$ and, in the case of the threshold of fluidization, it is equal to the particle settling velocity, Eq. (26), we determine the fluidization velocity as

$$u_{\mathrm{fluidization}} = \mathrm{Min}(\Phi v_t, u_{f,\mathrm{cr}}), \tag{28}$$

with terminal velocity $v_t$ from Eq. (3) and $u_{f,\mathrm{cr}}$ from Eq. (27). Figure 8 shows $u_{f,\mathrm{cr}}$ versus $\Phi$ from Eq. (27) and $\Phi v_t$ for fluid and particle parameters from Table V. As follows from this figure and Eq. (28), for $\Phi > 0.88$, the fluidization flow velocity is given by $\Phi v_t$.

An example of input and output parameters of the fluidization model is presented in Table V. In this table, $Q$ is the input ink volumetric flow, $S$ is the input cross-section of the channel, and $V_{\mathrm{flow}} = Q/S$ is the calculated ink flow velocity. Since the drag force on a stationary particle increases with an increase in the liquid flow velocity, in the case where $u_{\mathrm{fluidization}}$ is much smaller than $V_{\mathrm{flow}}$, the pigment particles will be moving with the liquid, while in the case where $u_{\mathrm{fluidization}}$ is larger than or about equal to $V_{\mathrm{flow}}$, pushing particles upwards through the vertical channel can be problematic.

## ACKNOWLEDGMENTS

The author would like to express his sincere gratitude to his colleagues Daniel Barnett and Matthew Aubrey for their kind support and helpful discussions during this research

**Table V.** Combined input and calculated parameters of the model.

| Input parameter | Input data |
|---|---|
| $D$ (m) | 5.00E-06 |
| $\rho_p$ (kg/m$^3$) | 1352 |
| $\rho_f$ (kg/m$^3$) | 1000 |
| $\mu$ (Pa · s) | 0.0150 |
| $\Phi$ — porosity | 0.80 |
| $C_1$ | 24.0 |
| $C_2$ | 1.2 |
| $Q$ (m$^3$/s) | 1.46E-08 |
| $S$ (m$^2$) | 9.0E-6 |
| **Output parameter** | **Output data** |
| $v_t$ (m/s) | 2.40E-7 |
| $u_{f,cr}$ (m/s) | 9.81E-8 |
| $u_{\text{fluidization}}$ (m/s) | 9.81E-8 |
| Recommended $u_{\text{ink}} = 5u_{\text{fluidization}}$ (m/s) | 4.91E-7 |
| $v_{\text{flow}}$ (m/s) | 1.62E-3 |

and would also like to thank Alexander Pekker for his kind help in preparation of the text of this article.

## APPENDIX

In this Section, we suggest an explanation of why the asymptote of the Shields curve, Eq. (11), obtained at relatively large $Re_*$, Fig. 1, can be extended to $Re_* \ll 1$. Following [8], the lift force applied to a spherical particle in a slow shear flow is

$$F_{\text{lift}} = 1.615\mu D^2 u_{sp}\sqrt{\frac{du}{dx}\mu\rho_f}, \tag{A1}$$

where $u_{sp}$ is the flow velocity far from the particle on the axis crossing the center of the particle and $du/dx$ is the gradient of the velocity, Figure A1.

In our case of a particle lying at the bottom of the channel, $u_{sp}$ can be written as

$$u_{sp} = \frac{du}{dx}\frac{D}{2}. \tag{A2}$$

In Eq. (A2), we have assumed a non-slip boundary condition at the wall. On substituting Eq. (A2) into Eq. (A1), we obtain

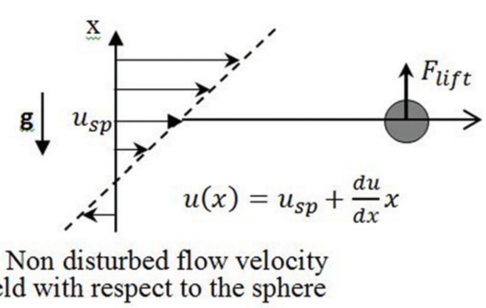


Figure A1. Illustration of model [8].

that, in our case, the lift force is

$$F_{\text{lift}} = \frac{0.81D^3\tau}{\mu}\sqrt{\tau\rho_f}. \tag{A3}$$

In Eq. (A3), we have substituted $du/dx$ from the expression for the shear stress, $\tau = \mu\, du/dx$. On substituting $du/dx$ into the creepy flow condition [8],

$$\sqrt{\frac{du}{dx}\frac{\rho_f}{\mu}}\frac{D}{2} \ll 1, \tag{A4}$$

and into Eq. (A2) and then using Eqs. (2) and (4), we obtain that the creepy flow condition [7], in the case of a particle lying at the bottom of the channel, reduces to the following form:

$$\frac{u_{sp}}{u_*} = \sqrt{\tau\rho_f}\frac{D}{2\mu} = \frac{Re_*}{2} \ll 1, \tag{A5}$$

which corresponds to the Shields diagram in the region of small $Re_*$. Thus, we have shown that, in the case of $Re_* \ll 1$, the use of Eq. (A3) for the lift force is quite reasonable. On setting Eq. (A3) equal to $\pi D^3 g(\rho_p - \rho_f)/6$, the gravitation force minus the bouncy force applied to the particle, we obtain a condition for the detachment of the particle from the bottom of the channel:

$$\tau_{*\,\text{det}} = \frac{0.65}{Re_*}. \tag{A6}$$

Thus, we have shown that both $\tau_{*\text{cr}}(Re_*)$, Eq. (11), and $\tau_{*\,\text{det}}(Re_*)$, Eq. (A4), are proportional of $1/Re_*$. The large difference in their coefficients is because the shear stress needed to initiate the sediment motion at the bed is much smaller than the shear stress required to lift a particle from the bed. Thus, regardless of such large differences in these coefficients, Eq. (A6) indicates that the Shields asymptote in Fig. 1 is applicable to laminar flows in microchannels (where $Re_* \ll 1$) as well.

## REFERENCES

[1] H. Rouse, "Modern conceptions of mechanics of fluid turbulence," Trans. ASCE **102**, 463–505 (1937).
[2] K. Whipple, (September 2004). "IV. Essentials of Sediment Transport" (PDF). *12.163/12.463 Surface Processes and Landscape Evolution: Course Notes*. MIT OpenCourseWare, Retrieved 2009-10-11.
[3] R. I. Ferguson and M. Church, "A simple universal equation for grain settling velocity," J. Sedim. Res. **74**, 933–937 (2004).
[4] A. Shields, *Anwedung der Aehnlichkeysmechanik und der Turbulenzforsschung auf die Geschiebebewegung* (Mitteilungen der Pruessischen Versuchanstalt fur Wasserbau und Schiffbau, Berlin, 1936), (uuid:61a19716-a994-4942-9906-f680eb9952d6).
[5] R. J. Garde and K. G. Ranga Raju, *Mechanics of Sediment Transportation and Alluvial Stream Problems*, 3rd ed. (New Age International, New Delhi, 2000).
[6] L. Pekker, *A calculator for Sediment Transport in Microchannels Based on the Rouse Number*, http://arxiv.org/abs/1712.07073.
[7] S. Ergum and A. A. Orning, "Fluid flow through packed columns," Chem. Eng. Prog. **48**, 89–94 (1952).
[8] P. G. Saffman, "The lift on small sphere in a slow shear flow," J. Fluid Mech. **22**, 385–400 (1965).